Effect of Wind Variability in the Emergency Reactive Support provided by Wind Farms

Theodoros Souxes
Giorgos Tzounas
Costas Vournas
School of Electrical and Computer Engineering
National Technical University of Athens
Athens, Greece
vournas@power.ece.ntua.gr

***Abstract*— This paper investigates the effect of Wind Farm (WF) active power variability on an emergency maximum reactive support control scheme. The latter is proposed as a means to increase the maximum power transfer, and thus the voltage stability limit of a weak transmission corridor. Substation and WF feeder controls (including switched capacitors and load tap changers), as well as converter current and voltage limitations are modelled in detail. Different case studies are examined to assess the impact of WF generation scenarios on the contribution of the emergency reactive support scheme on maximum power transfer.**

***Index Terms*— Reactive Power Control, Loadability Limit, Maximum Power Transfer, Wind Power, Voltage Stability.**

I. INTRODUCTION

Various applications aiming at providing support by distribution grids to the transmission system have been proposed in recent literature. In particular, the provision of reactive power from the distribution for the purpose of transmission system voltage control is an idea gaining momentum [1]-[3]. Since variable speed wind generators can control reactive power within the capabilities of their power electronic converters, they can play a significant role to the support of the main transmission system if appropriately controlled [4]-[6].

In previous work by the authors [7]-[8], the effect of reactive support by Wind Farms (WFs) to a weak transmission corridor was assessed assuming a constant active wind generation. As the available reactive support by the WF converter depends on active power flow, this paper focuses on the effect of variable wind power to the maximum power transfer (MPT) that can be achieved in the transmission corridor through the reactive support provided by WFs.

Two detailed medium voltage (MV) feeders corresponding to actual installations in the area of Peloponnese in the Hellenic Interconnected System are examined, using Quasi-Steady-State (QSS) simulation [9]. The impact of reactive support by the WF is assessed by computing the maximum power transfer provided to a remote load for different WF reactive control strategies. These include an Emergency Maximum Reactive Support (EMRS) control scheme based on a single command, issued when the transmission voltage falls below a pre-specified threshold [8].

The program (developed in Matlab) used to compute the increase in maximum active power transfer, when using the proposed EMRS control, is described in Section II.B. The variable wind time series used in the simulation are shown in Section II.C. The results are presented in Section III and IV for each of the two distribution feeders. Also, a test system where both WF feeders are connected simultaneously is examined in Section V, using constant wind generation. The system simulations in this Section are conducted using the QSS, long-term simulation program WPSTAB [10].

II. SINGLE WF TEST SYSTEM

A. Distribution MV Feeder Model and Controls

The first test system examined in this paper consists of a weak transmission corridor, in the middle of which a single WF is connected through a MV distribution feeder. The transmission corridor is represented by two equal reactances X on the source and load side respectively of the connection substation, as shown in Fig. 1 [8].

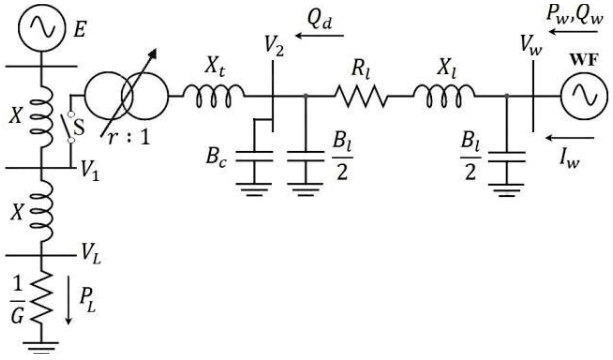

Figure 1. Complete Test system single-line diagram

As seen in Fig. 1, the transmission system is represented by a constant voltage source E, which is connected through the transmission corridor to a remote load. The load is connected to the load bus V_L and is considered as a variable conductance G with a unity power factor (i.e. it is assumed fully compensated).

Two specific distribution feeders of the Peloponnese network in Greece, WF#1 and WF#2 are considered. Both correspond to WFs equipped with variable speed generators. The detailed data for the two feeders, as well as the nominal ratings of the WFs are summarized in Table I [8]. It is noted that the two feeders have different features: WF#1 refers to a small park connected through a long MV line, while WF#2 is larger and is connected very close to the substation.

All the automatic controls of the feeder, i.e. switched capacitors B_C and Load Tap Changer (LTC) automatic control are simulated, as well as the active and reactive injection at the WF connection point.

TABLE I. TEST SYSTEM DATA

WF	Feeder Data (pu on S_B=100MVA)							
	Sn (MVA)	***E***	***X***	X_t	R_l	X_l	V_{lo}	r_o
#1	18.9	0.9703	0.2	0.4	0.431	1.0	0.972	0.99375
#2	36	0.9778	0.2	0.4	0.015	0.2	0.981	0.98750

The converter control is assumed instantaneous, i.e. it can operate multiple times without any time delay, in order to achieve the desired voltage and active power injection. The LTC control operates after the instantaneous converter control, whenever the distribution side voltage V_2 remains outside its narrow deadband for a time equal to the delay T_{LTC}. Tap ratio step Δr is constant and one tap change is performed each time, while the tap range is limited between r_{min}, r_{max} as in Table II.

Another discrete, but slower controller is assumed for the automatic switching of capacitor banks. To avoid adverse interactions, this controller objective is to keep the reactive power Q_d coming from the distribution feeder between 0 and a specified value Q^{band}. As shown in Table II, three switchable banks are connected to the HV/MV substation, each with a susceptance ΔB_c. The time delay before a capacitor bank switching T_{Bc} is assumed substantially larger, in order to avoid interactions with the LTC control [7], [8].

If during the simulation the WF current injection reaches the maximum current limit, the converter reactive control is changing the terminal voltage V_w in order to restore the current below the limit value I_{lim}.

The data of the reactive control mechanisms are summarized in Table II.

TABLE II. CONTROLLER DATA

r_{min}	r_{max}	Δr (%)	LTC steps	ΔB_c (MVAr)	B_c steps	T_{LTC} (s)	T_{Bc} (s)	Q^{band} (MVar)
0.8	1.1125	0.625	50	4	3	10	60	0-4

B. QSS System Simulation

The software package used for QSS system simulations and long-term stability analysis is developed in Matlab. It represents in detail the mechanisms, control devices and feeder data of Fig. 1 and Table I and II. The load conductance G is increased at every time step. In order to obtain maximum power transfer (MPT) conditions, a slow load admittance ramp with a 0.1% per second increase rate is simulated in discrete steps, until the system is past the MPT limit. The wind power (when variable) is also updated at each time step and as the controllers are all discrete, only algebraic equations need to be solved. The solution algorithm is briefly summarized below:

The WG active power P_w (which for variable wind is extracted as described in the next subsection) and the load conductance G are the system inputs. The terminal WF voltage V_w, depending on the reactive power control scheme simulated, the LTC tap r and the capacitor susceptance B_C form the state vector of the discrete system:

$$\boldsymbol{x} = [V_w, r, B_C]^{\mathrm{T}} \tag{1}$$

For each operating condition the values of (G, r, B_C) are given, thus the Thevenin equivalent seen from the MV bus of the WF can be constructed as seen in Fig. 2. It is noted that the WF voltage V_w depends on the reactive power control scheme simulated.

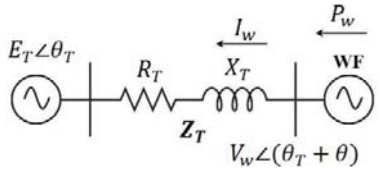

Figure 2. Thevenin Equivalent seen from the WF

For the configuration of Fig. 2 the angle θ can be directly determined solving the active power flow equation, as given in [11]:

$$P_W = \frac{E_T V_W}{Z_T} sin(\theta - \beta) + \frac{V_W^2}{Z_T^2} R_T \tag{2}$$

where $\beta=sin^{-1}(R_T/Z_T)$ is the loss angle of the Thevenin impedance $\mathbf{Z_T}$. All other variables, such as Q_w, I_w, etc. can be directly evaluated using circuit relationships after calculation of θ from (2).

C. Wind Farm Simulation with Variable Wind Speed

To simulate the effect of wind variability in the power transfer improvement, wind velocity time series are assumed as inputs to the wind generators. The sampling frequency of the time series equals to 1Hz. Two correlated wind speed time series are used for WF#1 and WF#2, with a total duration of 5000s.

In order to speed up the QSS simulation, the WF active power time series used as input to the model of Fig. 1 are extracted off-line using a variable speed wind generator model based on a doubly-fed asynchronous generator (DFAG) developed in Matlab/Simulink [12]. The DFAG model assumes symmetrical sinusoidal steady state neglecting the stator transients and stator resistance. Maximum power tracking control of the rotor speed is performed using typical vector control strategy. The turbine-generator shaft is represented by a two-mass model with inherent torsional damping. The wind power time series that result from the simulation of time series #1 and #2 are shown in Figs. 3 and 4 respectively. Since the wind speed remains below its nominal value, the pitch control remains inactive.

Coming back to the QSS model of the previous subsection, three control strategies for the WF converter reactive control are considered:

a) Unity Power Factor (UPF): the controller maintains a UPF, thus the WF voltage V_w changes in each time step to obtain Q_w=0.

b) Constant WF Voltage Control: wind farm voltage control is applied and as a result the reactive power Q_w is determined, so as to preserve the voltage constant.

c) Emergency Maximum Reactive Support (EMRS): the WF converter is modifying the voltage V_w to its maximum permissible value (1.10 pu in this study), when the primary voltage V_1 falls below a threshold. This is subject to the maximum current limitation of the converter.

The above control strategies consider variable wind power as input to the system, as shown in Figs. 3 and 4. The EMRS control described in case *c* is also simulated for two different scenarios of wind power generation. Constant wind power equal to low wind (case c_{low}) and constant wind power equal to high wind (90% of the rating, case c_{high}) are compared with the variable wind power scheme (case *c*).

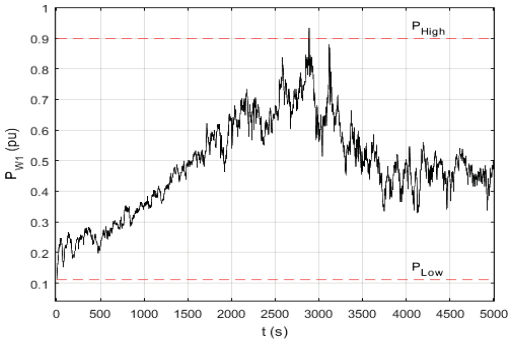

Figure 3. Wind Power Time Series of WF#1 (pu on S_{n1}=18.9 MVA)

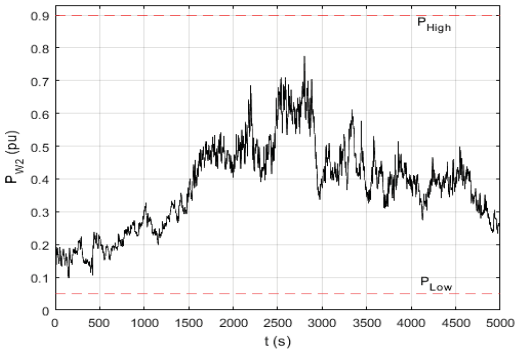

Figure 4. Wind Power Time Series of WF#2 (pu on S_{n2}=36 MVA)

III. WF#1 Results

A. Without Reactive Support

In order to compare the increase achieved in the MPT limit due to both WF feeder controls, the switch S of Fig. 1 is initially assumed open (base case), therefore, the distribution feeder is not connected to the transmission corridor. As a result, the MPT of the simplified two bus system according to [9], [11] is equal to:

$$P_{L_{max}} = \frac{E^2}{4X} \tag{3}$$

In Fig. 5, the load voltage is plotted for the base case and the UPF control (scheme *a*) as a function of the load consumed power. The simulation results seen in Fig. 5 are summarized in Table III. The WF#1 active power generation is the one of Fig. 3.

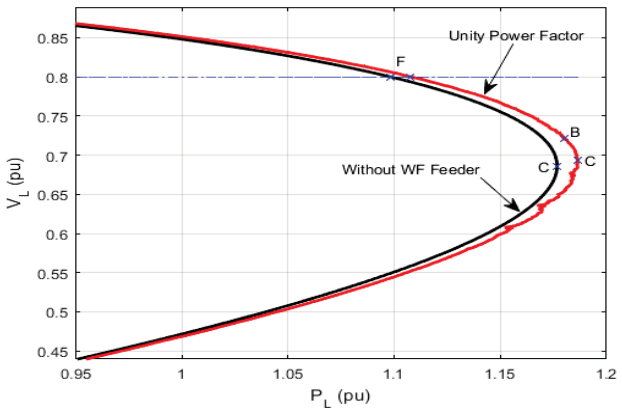

Figure 5. Load PV without WF Feeder and with Unity Power Factor curves (WF#1, Variable Wind Power)

Case (*a*) offers a small increase in system loadability with respect to the base case. The MPT in scheme (*a*) equals to 118.67MW, instead of 117.69MW. Point B corresponds to the time instant where the LTC tap ratio limit is reached, while point C indicates the maximum power transfer to the load bus.

At this point it should be noted that maximum power transfer is obtained at a low voltage level, as expected for a simple system, such as the one used here for the reactive support assessment.

If voltage constraints ($V \geq V_F$) are considered instead of the loadability point C in order to determine the power transfer, then this limit is obtained at point F, where $V=V_F$. The blue dashed line, shown in Figs. 5-10, indicates this transfer limit for V_F=0.8 pu.

B. Reactive Support Contribution

In this subsection, the EMRS control scheme (*c*) and the constant WF voltage control scenario (*b*) are simulated, in order to assess the impact of reactive support on the MPT limit. The results are also compared with case (*a*).

TABLE III. MPT WITH WF#1 (MW)

Variable Wind Power					
Without WF	***UPF* (*a*)**	***Constant WF Voltage* (*b*)**	***EMRS* (*c*)**	***ΔP Increase* (*c*)-base case**	
				(MW)	(%)
117.69	118.67	119.23	129.48	11.79	62.38
Emergency Maximum Reactive Support					
***Low P_w=2.1MW* (c_{low})**		***Variable P_w* (*c*)**		***High P_w=17MW* (c_{high})**	
130.07		129.48		128.81	

As seen in Fig. 6, which shows the load PV curve, and Table III, a 10.25MW load margin increase is achieved in case (*c*) with respect to (*b*) and 11.79MW with respect to base case, which is roughly 54% and 62% of the WF converter MVA rating respectively. Point E in Fig. 6 corresponds to the time instant of switching to maximum reactive support.

In the case of EMRS control, the increase achieved is significant, due to the maximum reactive support from the WF,

but also due to the automatic capacitors switching [8]. Reactive generation of WF#1 at maximum power transfer is equal to 8.62MVAr, while the injected reactive power at the HV bus is 16.38MVAr, taking into account also the capacitor contribution.

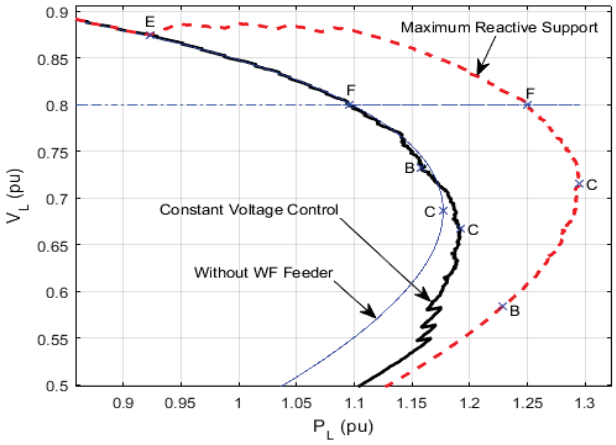

Figure 6. Load PV without WF Feeder, Constant Voltage and Maximum Reactive Support control curves (WF#1, Variable Wind Power)

C. *Effect of Variable Wind Power*

In this subsection, the effect of wind variability on the loadability limit, considering EMRS is examined. The consumed load power as a function of simulation time near the loadability limit is shown in Fig. 7 for variable wind power (as in Fig. 3) and with two constant wind power cases corresponding to low (case c_{low}) and high wind power (90% of the rating S_n, case c_{high}), both also shown in Fig. 3.

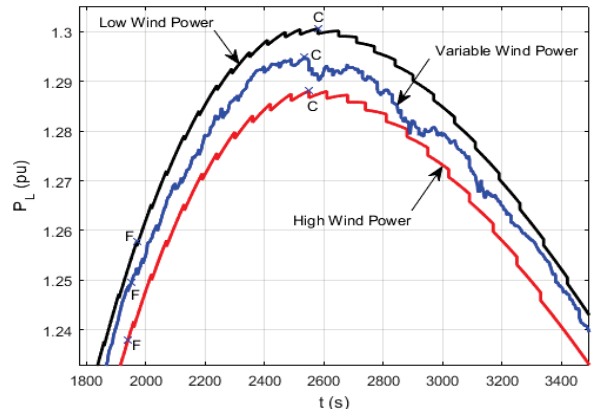

Figure 7. Load Power P_L for Low, High and Variable Wind Power Generation using Maximum Reactive Support Control (WF#1)

As noticed in Fig. 7 (and Table III concerning the limit), the two constant wind power cases enclose the variable wind power curve. As expected, for higher wind generation the system has lower MPT limit, due to the less available reactive support. However the difference between the two extreme cases considered is quite small. Thus, the wind variability in this case can be neglected and an average wind power can be used to calculate MPT with reasonable accuracy.

IV. WF#2 Results

A. *WF connection without Reactive Support*

The WF active power generation in this case is the time series seen in Fig. 4. Similar to the previous case, Fig. 8 shows the load PV curve computed from the simulation, while Table IV summarizes the results for the base case and unity power factor case (*a*). As seen, the WF connection with UPF offers a very small increase in system's loadability. The MPT for case (*a*) is 121.65MW, instead of 119.51MW in the base case.

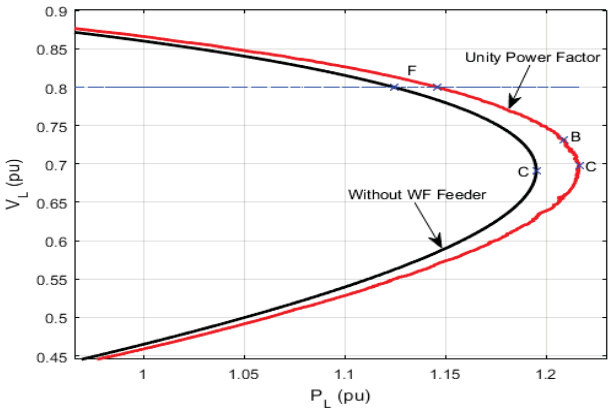

Figure 8. Load PV without WF Feeder and with Unity Power Factor curves (WF#2, Variable Wind Power)

B. *Reactive Support Contribution*

The EMRS control scheme (*c*) and the constant WF voltage control scenario (*b*) are simulated next for WF#2. As seen in the load PV curves of Fig. 9 and Table IV, a 15.65MW load margin increase is achieved comparing case (*c*) to case (*b*) and 23.52MW to base case, which is roughly 43% and 65% of the WF converter MVA rating respectively. Point D in Fig. 9 corresponds to the time instant when the maximum current of the WF converter is reached. It can be noticed that until the signal requesting maximum reactive support is issued (Point E), the same conditions apply (red dashed curve identical to black).

TABLE IV. MPT WITH WF#2 (MW)

Variable Wind Power					
Without WF	***UPF* (*a*)**	***Constant WF Voltage* (*b*)**	***EMRS* (*c*)**	***ΔP Increase* (*c*)-base case**	
				(MW)	(%)
119.51	121.65	127.38	143.03	23.52	65.33
Emergency Maximum Reactive Support					
***Low P_w=1.76MW* (c_{low})**		***Variable P_w* (*c*)**		***High P_w=32.4MW* (c_{high})**	
142.08		143.03		137.68	

As seen, the increase achieved by the EMRS is considerable. Reactive generation of WF#2 at maximum power transfer is equal to 33.36MVAr, while the injected reactive power in addition with the capacitor switching at the HV bus is 34.31MVAr.

Compared to the base case of disconnected WF feeder and the UPF case (*a*), the constant WF voltage control (case *b*) offers a bigger increase in the system loadability than in the case of WF#1. This is mostly due to the fact that two of the three capacitor banks are switched before the MPT point. As a result, the reactive power support from the WF is improved and thus, the maximum loadability limit is increased.

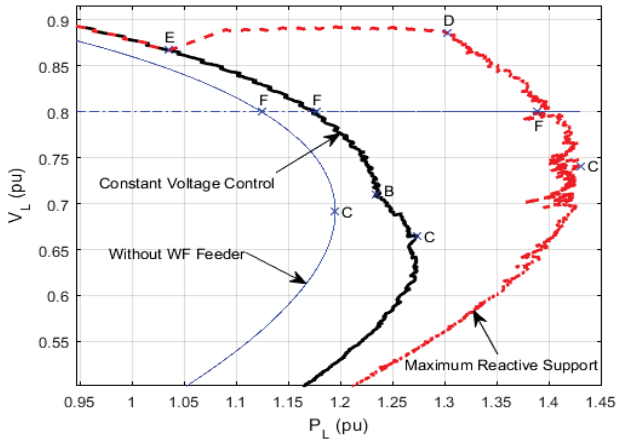

Figure 9. Load PV without WF Feeder, Constant Voltage and Maximum Reactive Support Control curves (WF#2, Variable Wind Power)

C. *Effect of Wind Power Variability*

The effect of wind variability with the EMRS control scheme in the maximum loadability is again compared to the two constant wind power scenarios (cases c_{high} and c_{low}) for wind power generation with high and low wind (all seen in Fig. 4).

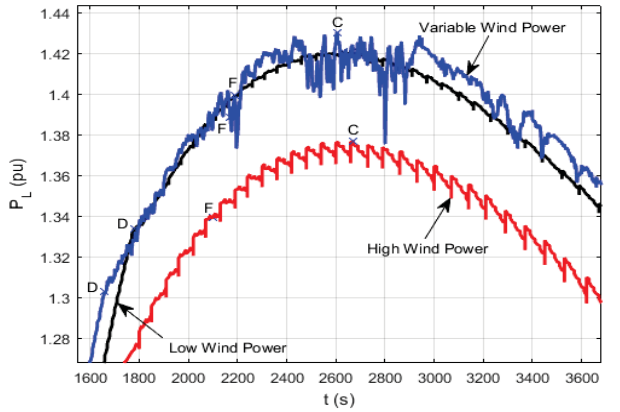

Figure 10. Load Power P_L for Low, High and Variable Wind Power Generation using Maximum Reactive Support Control (WF#2)

Figure 10 shows the consumed load power close to point C with constant and variable wind power. As seen in Fig. 10, in this case the two constant wind power curves do not enclose the variable wind power curve, as in the case of WF#1. The negative spikes appearing in Fig. 10, (e.g. P_L=137.56MW at t=2801s) occur when the value of the WF active generation increases abruptly (high spike of Fig. 4 at t=2801s). Note that at this time, the WF current limit has already been reached. Since the current limiter control is implemented by adjusting the voltage V_w of the WF, the WF voltage decreases in order to keep the current below its limit. As a result, the WF reactive support is reduced and thus the power transfer through the transmission corridor decreases due to the voltage drop.

As seen in Fig. 10 and Table IV, in this case the achieved power transfer with variable wind can be higher even from that obtained with constant low wind generation. However, as the sudden wind blasts can cause severe downward spikes in the consumption, it is safer to consider the MPT limit as that obtained for the constant high wind generation. In any case the difference is very small in the order of 5 MW.

V. System Simulation with both WFs

A. *System Description and Simulation Package*

In this section the simultaneous reactive support obtained from both WFs connected to different substation feeders of the same weak transmission corridor is examined and the effect on the MPT limit is assessed. The two WFs are considered to operate with constant low wind generation, thus the effect of wind variability, which was shown in the previous section to be rather small, is not considered here.

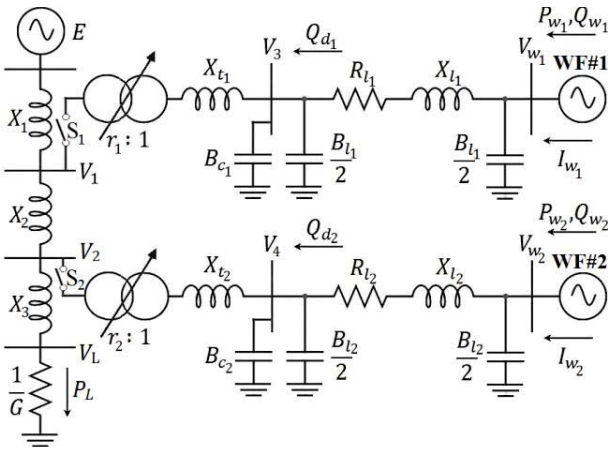

Figure 11. Complete Test system with both WFs connected

System simulation is conducted using the QSS, long-term simulation program WPSTAB [10] developed in NTUA. The test system is presented in Fig. 11 with data as in Table V.

TABLE V. Transmission Line Data (pu on 100MVA)

E	X_1	X_2	X_1
0.976	0.18	0.04	0.18

As seen, the total transmission line reactances remains the same as in system of Fig. 1 (0.4pu).

The automatic controls of the two feeders are the same and the same slow load admittance ramp is simulated, until the system is past the MPT limit.

B. *Simulation Results*

In order to compare the increase achieved in the MPT limit due to both WF feeder controls, the switches S_1 and S_2 of Fig. 11 are initially assumed open (base case). Again, case *b* corre-

sponds to the Constant WF Voltage Control and case *c* to the EMRS scheme.

As seen in Fig. 12, the MPT limit in the base case is 119.07MW, in case *b* 130.86MW and in case *c* 153.63MW. The achieved load margin increase with respect to the base case is summarized in Table VI in MW, as well as in percent of the sum of the two WF converter MVA ratings. Note that the total support from WF #1 and WF#2 in terms of MPT increase, is similar to that of each WF separately.

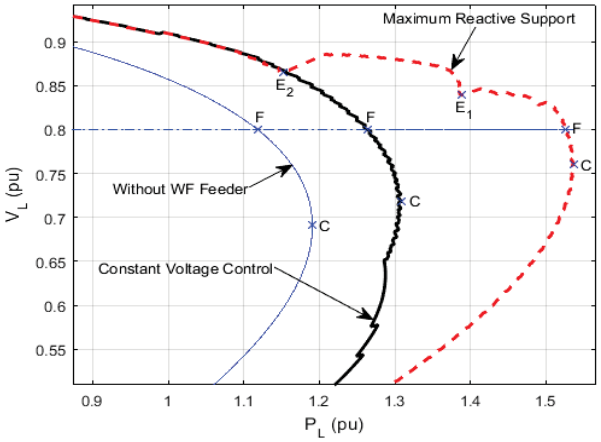

Figure 12. Load PV without WF Feeder, Constant Voltage and Maximum Reactive Support Control curves (Both WFs, Low Wind Power)

TABLE VI. MPT INCREASE IN REACTIVE CONTROL SCHEMES (LOW P_W)

	Base Case	***Constant WF Voltage (b)***		***EMRS (c)***	
	(MW)	(MW)	(%)	(MW)	(%)
WF #1	117.69	3.54	18.73	12.38	65.50
WF #2	119.51	9.46	26.28	22.57	62.69
Both WFs	119.07	11.79	21.48	34.56	62.95

C. Power Transfer limit with voltage constraints

Finally, in Table VII the maximum power transfer results considering low-voltage limit constraint are shown for variable wind power, as discussed in Section III.A. The results are summarized for both WFs and low wind power. Note that the effect on maximum transfer is similar to that obtained, when considering maximum loadability without low-voltage constraints. Thus, reactive support from the WFs will provide increase in loadability regardless of the imposition of low-voltage constraints.

TABLE VII. POWER TRANSFER LIMITS (MW) WITH LOW-VOLTAGE CONSTRAINTS

WF	***Without WF***	***UPF (a)***	***Constant WF Voltage (b)***	***EMRS (c)***	***ΔP Increase (c)-base case***	
					(MW)	(%)
#1	109.82	110.78	109.54	124.96	15.14	80.11
#2	112.45	114.62	117.72	138.86	26.41	73.36
Both	111.82	112.63	126.31	152.41	40.59	73.93

VI. CONCLUSIONS

In this paper the effect of emergency reactive support obtained from two WFs connected to MV feeders was examined. This support was quantified in terms of the obtained increase in maximum power transfer to a remote load fed by the transmission system. The effect of wind variability in this emergency support was also investigated. In all cases the MPT was increased considerably using the proposed emergency control, while the effect of wind variability was rather minor, even though it did affect power transfer particularly when the converter operates under current control at its maximum rating. In all cases it is safe to assume high wind power when assessing the effect of reactive support. It is noted however that the case of fully loaded converters was not considered, with the high wind generation case being at 90% of converter rating.

The most interesting conclusion of this study is that despite the difference in the dedicated MV feeder structure (small or long line, either each one separately or both connected simultaneously) the contribution to the increasing MPT is similar in all cases, and always above 60% of the total installed capacity of the WFs. This feature allows a rough estimate of the achieved support, of course for the examined transmission corridor. This feature is very encouraging for future applications of the proposed EMRS scheme.

REFERENCES

[1] M. Zerva and M. Geidl, "Contribution of active distribution grids to the coordinated voltage control of the swiss transmission system," *2014 Power Systems Computation Conference*, Wroclaw, 2014, pp. 1-8.

[2] S. Mat Zali and J. V. Milanović, "Generic Model of Active Distribution Network for Large Power System Stability Studies," in *IEEE Transactions on Power Systems*, vol. 28, no. 3, pp. 3126-3133, Aug. 2013.

[3] P. Aristidou, G. Valverde and T. Van Cutsem, "Contribution of Distribution Network Control to Voltage Stability: A Case Study," in *IEEE Transactions on Smart Grid*, vol. 8, no. 1, pp. 106-116, Jan. 2017.

[4] P. Pourbeik, convenor WG C4.601, "Modeling and dynamic behavior of wind generation as it relates to power system control and dynamic performance", CIGRE Technical Brochure 328, Section 6, Aug. 2007

[5] D. F. Opila, A. M. Zeynu and I. A. Hiskens, "Wind farm reactive support and voltage control," *2010 IREP Symposium Bulk Power System Dynamics and Control - VIII (IREP)*, Rio de Janeiro, 2010, pp. 1-10.

[6] J. Zhai and H. Liu, "Reactive power control strategy of DFIG wind farms for regulating voltage of power grid," *2014 IEEE PES General Meeting | Conference & Exposition*, National Harbor, MD, 2014, pp. 1-5.

[7] C. Vournas, C. Lambrou, I. Anagnostopoulos, G. Christoforidis and J. Kabouris, "Distributed reactive support and voltage stability limits: The example of Peloponnese in the Hellenic Interconnected System," *2015 IEEE PES General Meeting*, Denver, CO, 2015, pp. 1-5.

[8] C. Vournas, I. Anagnostopoulos, T. Souxes, "Transmission support using Wind Farm controls during voltage stability emergencies", *Control Engineering Practice*, vol. 59, pp. 100-110, Feb. 2017.

[9] T. Van Cutsem, C. Vournas, *Voltage stability of electric power systems*, Kluwer Academic Publishers, 1998, Springer 2008.

[10] C. D. Vournas, G.A. Manos, J. Kabouris and T. Van Cutsem, "Analysis of a voltage instability incident in the Greek power system," *2000 IEEE PES Winter Meeting Conference Proceedings*, pp.1483-1488 vol.2, 2000

[11] C. Vournas, "Maximum Power Transfer in the Presence of Network Resistance," in *IEEE Transactions on Power Systems*, vol. 30, no. 5, pp. 2826-2827, Sept. 2015.

[12] G. Tsourakis and C. Vournas, "Modelling, control and stability of wind turbines with doubly fed induction generator", Proceedings of *CIGRE Symposium Power Systems with Dispersed Generation*, Athens, Greece, 13-16 April 2005.